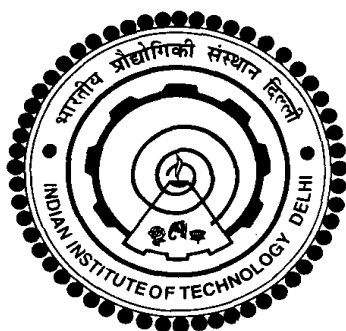


**METAL AND METAL OXIDE NANOCOMPOSITES FOR  
EFFICIENT ELECTROCATALYTIC AND MAGNETIC PROPERTIES**

**BHARAT KUMAR**



**DEPARTMENT OF CHEMISTRY  
INDIAN INSTITUTE OF TECHNOLOGY, DELHI  
INDIA  
MAY, 2015**

© Indian Institute of Technology Delhi (IITD), New Delhi, 2015

**METAL AND METAL OXIDE NANOCOMPOSITES FOR  
EFFICIENT ELECTROCATALYTIC AND MAGNETIC PROPERTIES**

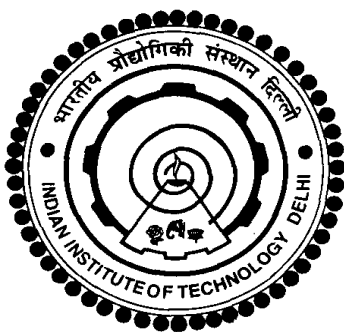
By

**BHARAT KUMAR**

**Department of Chemistry**

Submitted in fulfillment of the requirements for the Degree of Doctor of  
Philosophy

to the



**INDIAN INSTITUTE OF TECHNOLOGY, DELHI**

**INDIA**

**MAY, 2015**

*Dedicated to my  
Parents and  
Supervisor*

## CERTIFICATE

This is to certify that the thesis entitled, “**Metal and metal oxide nanocomposites for efficient electrocatalytic and magnetic properties**” being submitted by **Mr. Bharat Kumar** to the Indian Institute of Technology, Delhi for the award of the degree of **Doctor of Philosophy** in Chemistry, is a record of bonafide research work carried out by him. Mr. Bharat Kumar has worked under my guidance and supervision, and has fulfilled the requirements for the submission of this thesis, which to my knowledge has reached the requisite standard.

The results contained in this dissertation have not been submitted in part or full, to any other university or institute for award of any degree or diploma.

**Date:**

**Professor A. K. Ganguli**

Department of Chemistry

Indian Institute of Technology, Delhi

New Delhi – 110016, INDIA

## **Acknowledgements**

Looking back I am surprised at how quickly time has elapsed and how I have completed my five years of stay at IIT Delhi for my Ph.D. I am very grateful for all I have received throughout these years. It is a great pleasure to extend my heartfelt regards to all those who made this thesis possible. It has certainly shaped me as a person and has led me to where I am now.

First of all, I would like to express my deep sense of gratitude and regards to my supervisor Prof. A. K. Ganguli (my Guru), Director, Institute of Nano Science and Technology, Mohali, and Professor at Department of Chemistry, IIT Delhi for his valuable guidance, scholarly inputs and consistent encouragement. But for the confidence he instilled in me this feat of completing my Ph.D. would have been impossible. Prof. Ganguli has enlightened me through his wide knowledge and his deep intuition and has always been available to clarify my doubts. With his inspiration, enthusiasm, great efforts, and excellent guidance during my Ph.D. tenure, I could avail the right opportunities to grow as a researcher as well as an individual. Throughout, my Ph.D. and thesis-writing period, he provided encouragement, sound advice, good teaching, good company, and lots of good ideas. He has always brought out the best in me, and this period of working with him has been a wonderful learning experience and hence I am very thankful for all he has done for me. I shall never forget the caring gesture of Sir when I fractured my leg. He is used to pick and drops me in hostel.

I am grateful to Dr. P. K. Chowdhury for extending his help and cooperation especially during absence of my research supervisor.

I am grateful to the former head Prof. A. K. Singh and present head Prof. A. Ramanan of Department of Chemistry for providing me all necessary facilities in the department. I am

also grateful to all faculty and supporting staff of the department for their kind help and cooperation.

I would like to express my special regards to Mrs. Jaya Ganguli for her support and affection received during my stay at IIT Delhi. She was one of them who encouraged me a lot towards the steps of successful work.

I express my sincere thanks to Prof. K. V. Ramanujachary and Prof. S. E. Loafland, Rowan University, U.S.A. for the magnetic measurements and their valuable suggestions. I also wish to thank Prof. R. Chatterjee, Department of Physics, IIT Delhi for the magnetic measurements.

I would also like to thank IIT Delhi for providing me platform and fellowship, which has supported me during my entire research period.

I express my sincere thanks to my former and present lab-colleagues, especially Dr. Tokker, Dr. Vishnu, Dr. Saroj, Dr. Sonalika, Dr. Jahangeer, Dr. Jai Prakash, Dr. Aparna, Dr. Menaka, Dr. Aditya, Dr. Debashree, Dr. Sunita, Dr. Soma, Dr. Mrinmoyee, Dr. Ashima, Dr. Masood Nath, Dr. Manu, Dr. Sharmila, Dr. Parthsarathi, Dr. Anjenellu, Gohil, Kasinath, Soumen, Nibedita, Neha, Arabinda, Sandeep, Zeba, Vaishali, Nitin, Vandana, Sanjit, Jayanti and Anil for their love, understanding and providing an excellent working environment.

I fall short of words to express my feelings for my grandfather Late Sri Nand Kishor Chaubey, my father Sri Onkar Nath Chaubey and my mother Smt. Chameli Chaubey for their constant motivation, inspiration, support, understanding and love. But for their blessings it would not have been possible to complete my work smoothly.

Words cannot express my feelings towards my loving brothers and sister (Ram Chandra, Shatrughan, Brij, Urmila, Mandavi and Sharda) who have done everything to enable me to concentrate on my research single-mindedly and their love, support and faith. I would like to

thank my bhabhi for her love, care, support and my niece & nephew for their love and affection.

I fall short of words to express my feelings for my wife Nitu Tiwari Chaubey for her love, inspiration and support. I have always found her standing by me in toughest phase of my life. She has been a source of strength and courage to me. Thanks Nitu for being with me. I thank my father-in-law (Sri B. N. Tiwari) and mother-in-law (Mrs. Maya Tiwari) for their love, support.

Special thanks to Dr. G. K. Rao for his unconditional support. He is the person who always stood by me. Gyan sir thanks for being my senior and brother.

I sincerely appreciate and reciprocate the warm-heartedness, goodwill and love of my friends, especially, Amar, Arvind, Birader, Brijesh, Dinesh, Gyan, Sachin, Santosh, Shulka and Vikas. Birader was always available to me for scientific discussion. I have always found my friend standing by me in difficulties. Thanks Amar, Brijesh, Gayn and Sachin for the good care you took of me during the toughest time of my life. I fall short of words for Brijesh who inspite his busy schedule of IAS main examinations took care of me.

I express my sincere thanks to all Jwalamukhi hostel resident, house master, warden and staff for providing me nice company during my hostel living period. It is like my home where I had enjoyed the moment which will be unforgettable to entire life.

Last, but not the least, I thank the Almighty for gifting me the life with such wonderful people. Without His blessings, this thesis would certainly have not been successfully completed.

**Bharat Kumar**

## ABSTRACT

Energy resources and environmental issues are the two important topics of concern at present global level scenario. To effectively address these issues, there has been extensive research for technologies that provide energy and help in environmental remediation that is a renewable, safe, clean, cheap and viable alternative to fossil fuels. To meet the energy demand, materials are designed to capture solar energy and new renewable energy. It is universally accepted that hydrogen is one of the best energy source because it can be used as clean fuel (by product is  $H_2O$ ) in a variety of energy sectors including the conversion to electricity without  $CO_2$  emission, producing  $CH_4$  by absorbing  $CO_2$  from the environment. One of the potential ways to combat these present energy and environmental crises will be electrocatalysis and photocatalysis. Water splitting reaction, hydrogen evolution reaction (HER) and oxygen evolution reaction has been a growing interest in search of materials with electrocatalytic and photocatalytic properties. Metal and metal oxides based electrocatalyst & photocatalysts have been proven to be potentially advantageous for splitting of water to supply clean and recyclable hydrogen energy as well as environmental pollutant remediation for complete decomposition of organic compounds into  $H_2O$  and  $CO_2$  at ambient conditions. Also, the magnetic nanostructured materials are of intense interest due to their potential use in magnetic resonance imaging, biomedicine, data storage and environmental remediation. The new materials are being explored and examined in order to meet all these requirements for electrocatalytic and magnetic applications.

The design of nanostructured metal and metal oxide based materials has become one of the most challenging fields of nanoscience and technology due to its unique properties and important applications in catalysis, electronics and photonic devices. Due to the small sizes

and large surface area, of nanosized materials are known to have unique features in high reactivity and enhanced catalytic activity.

*So, the motivation of the present thesis is to develop alternate approaches for the synthesis of nanostructured metal, metal oxide and their nanocomposites to investigate their electrocatalytic properties and to establish factors influencing the efficiency of catalysis. The magnetic properties of materials have importance in magnetic resonance imaging, biomedicine, data storage and environmental remediation.*

In the present investigation, we focus our study on the enhancement of the efficiency of electrocatalysts and magnetic materials (metal, metal oxide and composites) with the control of size, morphological features, and surface area by increasing the surface/volume ratio. These nanomaterials were synthesized by coprecipitation, hydrothermal and microemulsion methods under varying reaction conditions. Such size and shape tunable materials have the potential to enhance the production of hydrogen and oxygen as well as magnetic properties. This thesis deals with the synthesis, characterization, electrocatalytic (HER & OER) and magnetic properties of various metal, metal oxide nanostructures and composites.

Chapter 1 deals with the detailed survey of the literature background of metal and metal oxide in the area relevant interesting electrocatalytic and magnetic properties. We also discuss various possibilities of synthetic process for obtaining metal, metal oxide in bulk as well as nano regime. The details of characterization techniques, basics of electrocatalytic (HER & OER), magnetic and photocatalytic properties have been discussed.

In chapter 2, copper oxalate nanorods were synthesized by modified microemulsion method. Using copper oxalate and CuO, we have synthesized Cu, Cu<sub>2</sub>O nanoparticles and Cu/Cu<sub>2</sub>O nanocomposites at 350 °C. These materials were characterized with various

characterization techniques such as FESEM, TEM and XPS. The hydrogen and oxygen evolution reaction have been carried out using these electrocatalysts in which Cu/Cu<sub>2</sub>O nanocomposites are more efficient than Cu & Cu<sub>2</sub>O for HER as well as OER. These electrocatalyst are very stable over 50 cycles of electrocatalysis. Photocatalytic degradation of Methylene blue is also carried out by using Cu<sub>2</sub>O which show 98 % degradation of Methylene blue dye in visible light.

Chapter 3 deals with the morphology based synthesis of Cu/Cu<sub>2</sub>O nanocomposites by one step hydrothermal method at different reaction times (24, 72, 120 h). The study of role of reaction time is to see the effect on growth of particles inside the hydrothermal reaction as well as on the reduction of Cu<sup>2+</sup> to Cu<sup>+</sup> & Cu<sup>0</sup>. The TEM studies show the morphology varying from nanorods at higher reaction time to agglomerated nanoparticles at lower reaction time. The nanorods shape Cu/Cu<sub>2</sub>O nanocomposites produce higher current in hydrogen & oxygen evolution reaction (amount of H<sub>2</sub> and O<sub>2</sub>) as compared to assemble nanoparticles (72 h) and agglomerated (24 h) nanoparticles. Sonogashira cross couple product was also higher in case of rod shaped morphology.

In chapter 4, the synthesis nano-micron (n-μ) composites of CuO by mixing of the micron sized CuO and copper oxalate at 350 °C and their characterization by powder X-ray diffraction, diffuse reflectance spectroscopy, transmission electron microscopy and surface area measurements along with hydrogen evolution reaction and magnetic properties have been discussed. It was observed that pure nano sized particles produce more current density as compared to pure micron sized particles and nano-micron composites due to more surface area and alignment of the nanoparticles. The highest and lowest magnetizations were found for pure nano and micron sized CuO respectively.

In chapter 5, the synthesis of Co nanoparticles (from cobalt oxalate obtained by reverse micellar method) with varying size and their electrocatalytic & magnetic properties is discussed. It is observed that as the heating rate was slower, the size of nanoparticles was smaller which produce more H<sub>2</sub> and O<sub>2</sub> due to higher surface area (more active site) as compared to higher heating rate synthesis methodology. The magnetization value was the opposite. The smaller size of nanoparticles has lower saturation magnetization value.

In chapter 6, we discuss about the synthesis of BaTiO<sub>3</sub> obtained by hydrothermal route and CoFe<sub>2</sub>O<sub>4</sub> by coprecipitation as well as by hydrothermal route. The heterostructures of BaTiO<sub>3</sub>@CoFe<sub>2</sub>O<sub>4</sub> were synthesized by four different reaction protocols and it named as CS1, CS2, CS3 and CS4. The TEM study shows the variation of morphology as well as particles size of the above synthesized materials. The magnetic study of these CoFe<sub>2</sub>O<sub>4</sub> nanoparticles and heterostructures of BaTiO<sub>3</sub>@CoFe<sub>2</sub>O<sub>4</sub> was carried out which show the ferromagnetic behavior at 100 as well 300 K. The coercivity, saturation magnetization and remnant magnetization of these materials were calculated and compared with each other. CS4 have lowest coercive field value at 100 and 300 K whereas the CS3 has the highest magnetization value.

Chapter 7 discusses the synthesis of nano-micron (n-μ) composites of La<sub>0.82</sub>Sr<sub>0.18</sub>MnO<sub>3</sub> by mixing the micron sized La<sub>0.82</sub>Sr<sub>0.18</sub>MnO<sub>3</sub> and nano sized La<sub>0.82</sub>Sr<sub>0.18</sub>MnO<sub>3</sub> at 1200 °C in air. The density of these nano-micron composites was found to be 95 to 99 % of the theoretical density. The entire series of the La<sub>0.82</sub>Sr<sub>0.18</sub>MnO<sub>3</sub> shows ferromagnetic behavior. The enhancement in the saturation magnetization (30%) is observed on addition of~ 1.0 weight percent of nanoparticles of La<sub>0.82</sub>Sr<sub>0.18</sub>MnO<sub>3</sub> to micron-size La<sub>0.82</sub>Sr<sub>0.18</sub>MnO<sub>3</sub>.

In Chapter 8, conclusions and future prospects of the work described in the thesis have been discussed. The low temperature methodologies have been developed using microemulsion and hydrothermal mediated precursors to obtain various morphologies of nanostructured metal and metal oxide based materials. The synthesis temperature was lowered by 200°C to 400°C in metal and metal oxides by the above reaction protocol.

We suggest metal and metal oxide system which may be pursued for both basic scientific interest and attractive applications in near future. These nanomaterials have sufficient research interest to a variety of researchers working on fuel cells, batteries, nanocapacitors, memory devices etc.

## TABLE OF CONTENTS

CERTIFICATE		i
ACKNOWLEDGEMENTS		ii
ABSTRACT		v
TABLE OF CONTENTS		x
LIST OF FIGURES		xviii
LIST OF TABLES		xxix
ABBREVIATIONS AND SYMBOLS		xxxix
<b>CHAPTER 1</b>	<b>Introduction</b>	
1.1	Introduction	2
1.2	Synthesis of nanomaterials	4
1.3	Characterization techniques	14
1.4	Properties of materials	24
1.4.1	Magnetic properties	24
1.4.2	Electrocatalytic properties	28
1.4.3	Photocatalytic property	34
1.5	Motivation of the thesis	39
1.6	References	41
<b>CHAPTER 2</b>	<b>Synthesis, characterization and electrocatalytic properties of Cu &amp; Cu<sub>2</sub>O nanoparticles and Cu/Cu<sub>2</sub>O nanocomposites</b>	
2.1	Introduction	49
2.2	Experimental	52

2.2.1	Materials	52
2.2.2	Preparation of copper oxalate	52
2.2.3	Preparation of copper metal (Cu) nanoparticles	53
2.2.4	Preparation of cuprous oxide (Cu <sub>2</sub> O) nanoparticles	53
2.2.5	Preparation of copper/cuprous oxide (Cu/Cu <sub>2</sub> O) nanocomposites	53
2.2.6	Schematic representation of the synthesis methodology	54
2.3	Characterization of materials	54
2.3.1	Powder x-ray diffraction	54
2.3.2	Thermogravimetric analysis and differential scanning calorimetry	55
2.3.3	Field emission scanning electron microscopy	55
2.3.4	Transmission electron microscopy	55
2.3.5	BET surface area	55
2.3.6	XPS Measurements	56
2.3.7	Diffuse-reflectance spectroscopy	56
2.3.8	Electrochemical measurements	56
2.3.9	Photocatalytic measurements	57
2.4	Results and discussion	58
2.4.1	X-ray study and analysis	58
2.4.2	Thermogravimetric, differential thermal analysis and differential scanning calorimetry study and analysis	62
2.4.3	Field emission scanning electron microscopy study and analysis	64
2.4.4	Transmission electron microscopy study and analysis	66
2.4.5	XPS study and analysis	70
2.4.6	BET surface area study and analysis	71

2.4.7	Diffuse reflectance spectra study and analysis	71
2.4.8	Hydrogen evolution reaction study and analysis	72
2.4.9	Oxygen evolution reaction study and analysis	75
2.4.10	Stability of electrocatalyst after HER and OER study and analysis	78
2.4.11	Photocatalytic study and analysis	81
2.5	Conclusions	89
2.6	References	90

**CHAPTER 3      Morphological evolution from spherical nanoparticles to core shell nanorods of Cu/Cu<sub>2</sub>O nanocomposites obtained by hydrothermal route and their properties**

3.1	Introduction	98
3.2	Experimental	100
3.2.1	Materials	100
3.2.2	Synthesis of copper/cuprous oxide (Cu/Cu <sub>2</sub> O) nanocomposites	100
2.3	Characterization of materials	101
2.3.1	Powder X-ray diffraction	101
3.3.2	Transmission electron microscopy	101
3.3.3	BET surface area	102
3.3.4	Diffuse-reflectance spectroscopy	102
3.3.5	Electrochemical measurements	102
3.3.6	Sonogashira cross-coupling reaction	103
3.4	Results and discussion	103
3.4.1	X-ray study and analysis	103

3.4.2	Transmission electron microscopy study and analysis	105
3.4.3	BET surface area study and analysis	108
3.4.4	Diffuse reflectance spectroscopy study and analysis	110
3.4.5	Cyclic voltammetry study and analysis	111
3.4.6	Electrochemical impedance spectroscopy study and analysis	114
3.4.7	Sonogashira cross-coupling reaction study and analysis	115
3.5	Conclusions	118
3.6	References	119

**CHAPTER 4      Nano – micron composites of CuO and their electrocatalytic & magnetic properties**

4.1	Introduction	125
4.2	Experimental	127
4.2.1	Materials	127
4.2.2	Preparation of copper oxalate	127
4.2.3	Preparation of copper oxide nano – micron composites	127
4.3	Characterization of materials	128
4.3.1	Powder x-ray diffraction (PXRD)	128
4.3.2	Field emission scanning electron microscopy (FESEM)	129
4.3.3	Transmission electron microscopy (TEM)	129
4.3.4	BET surface area	129
4.3.5	Density measurements	129
4.3.6	Diffuse-reflectance spectroscopy (DRS)	130
4.3.7	Electrochemical measurements	130

4.3.8	Magnetic measurement	130
4.4	Results and discussion	131
4.4.1	X-ray study and analysis	131
4.4.2	Field emission scanning electron microscopy study and analysis	132
4.4.3	Transmission electron microscopy study and analysis	135
4.4.4	BET Surface area study and analysis	138
4.4.5	Density study and analysis	139
4.4.6	Diffuse reflectance spectroscopy study and analysis	139
4.4.7	Hydrogen evolution reaction study and analysis	140
4.4.8	Magnetic property study and analysis	144
4.5	Conclusions	150
4.6	References	151
<b>CHAPTER 5</b>	<b>Synthesis, characterization, electrocatalytic and magnetic properties of Co nanoparticles</b>	
5.1	Introduction	158
5.2	Experimental	160
5.2.1	Materials	160
5.2.2	Preparation of cobalt oxalate nanorods	160
5.2.3	Preparation of cobalt metal (Co) nanoparticles	160
5.3	Characterization of materials	161
5.3.1	Powder x-ray diffraction	161
5.3.2	Thermogravimetric analysis and differential scanning calorimetry	161
5.3.3	Field emission scanning electron microscopy	161

5.3.4	Transmission electron microscopy	161
5.3.5	BET surface area	161
5.3.6	Electrochemical measurements	162
5.3.7	Magnetic measurements	162
5.4	Results and discussion	163
5.4.1	X-ray study and analysis	163
5.4.2	Thermogravimetric, differential thermal analysis and differential scanning calorimetry study and analysis	165
5.4.3	Field emission scanning electron microscopy and transmission electron microscopy study and analysis	166
5.4.4	BET surface area study and analysis	168
5.4.5	Hydrogen evolution reaction study and analysis	169
5.4.6	Oxygen evolution reaction study and analysis	171
5.4.7	Electrochemical impedance spectroscopy study and analysis	173
5.4.8	Magnetic properties study and analysis	174
5.5	Conclusions	177
5.6	References	178
<b>CHAPTER 6</b>	<b>CoFe<sub>2</sub>O<sub>4</sub>, BaTiO<sub>3</sub> nanoparticles and BaTiO<sub>3</sub>@CoFe<sub>2</sub>O<sub>4</sub> heterostructures</b>	
6.1	Introduction	185
6.2	Experimental	187
6.2.1	Materials	187
6.2.2	Synthesis of cobalt ferrite (CoFe <sub>2</sub> O <sub>4</sub> )	187

6.2.3	Synthesis of barium titanate (BaTiO <sub>3</sub> )	188
6.2.4	Synthesis of barium titanate/cobalt ferrite (BaTiO <sub>3</sub> /CoFe <sub>2</sub> O <sub>4</sub> ) heterostructures by coprecipitation/hydrothermal functionalization route	189
6.2.5	Synthesis of barium titanate/cobalt ferrite(BaTiO <sub>3</sub> /CoFe <sub>2</sub> O <sub>4</sub> ) heterostructures by in-situ hydrothermal route	191
6.3	Characterization of materials	192
6.3.1	Powder x-ray diffraction	192
6.3.2	Field emission scanning electron microscopy	192
6.3.3	Transmission electron microscopy	192
6.3.4	BET surface area	193
6.3.5	Magnetic measurements	193
6.4	Results and discussion	193
6.4.1	X-ray study and analysis	193
6.4.2	Field emission scanning electron microscopy study and analysis	199
6.4.3	Transmission electron microscopy study and analysis	203
6.4.4	BET surface area study and analysis	210
6.4.5	Magnetic properties study and analysis	212
6.5	Conclusions	216
6.6	References	217
<b>CHAPTER 7</b>	<b>Nano – micron composites of GMR materials, La<sub>0.82</sub>Sr<sub>0.18</sub>MnO<sub>3</sub></b>	
7.1	Introduction	224
7.2	Experimental	225

7.2.1	Materials	225
7.2.2	Preparation of $\text{La}_{0.82}\text{Sr}_{0.18}\text{MnO}_3$ micron sized particles	226
7.2.3	Preparation of $\text{La}_{0.82}\text{Sr}_{0.18}\text{MnO}_3$ nano sized particles	226
7.2.4	Preparation of nano-micron composites of $\text{La}_{0.82}\text{Sr}_{0.18}\text{MnO}_3$	227
7.3	Characterization of materials	228
7.3.1	Powder x-ray diffraction	228
7.3.2	Transmission electron microscopy	228
7.3.3	Field emission scanning electron microscopy	228
7.3.4	Density measurements	229
7.3.5	BET surface area	229
7.3.6	Magnetic measurement	229
7.4	Results and discussion	229
7.4.1	X-ray study and analysis	229
7.4.2	Transmission electron microscopy study and analysis	233
7.4.3	Field emission scanning electron microscopy study and analysis	233
7.4.4	Energy dispersive X-ray study and analysis	237
7.4.5	Density and surface area study and analysis	239
7.4.6	Magnetic properties study and analysis	241
7.5	Conclusions	245
7.6	References	246
<b>CHAPTER 8</b>	<b>Conclusions and scope for further research</b>	<b>249</b>
	<b>Bio-Data of the Author</b>	<b>255</b>

## LIST OF FIGURES

Figure No.	Figure Captions	Page No.
Figure 1.1	Schematic diagram of autoclave used for hydrothermal reaction	8
Figure 1.2	Structure of reverse micelle	9
Figure 1.3	Mechanism of the formation of nanoparticles in microemulsions	11
Figure 1.4	Structure of surfactant	12
Figure 1.5	X-ray diffraction based on the principle of Bragg's	14
Figure 1.6	Various processes involved with interaction of electrons with a sample	23
Figure 1.7	Magnetic hysteresis loop of a ferromagnetic substance	25
Figure 1.8	Temperature dependent behavior of (a) paramagnetic (b) ferromagnetic (c) antiferromagnetic substances	26
Figure 1.9:	Plot of reciprocal susceptibility vs temperature for Curie and Curie-Weiss Law	27
Figure 1.10	Three electrode system of cyclic voltammetry	28
Figure 1.11	The basic two electrode working electrochemical cell	29
Figure 1.12	A typical cyclic voltammogram for reversible reaction	31
Figure 1.13	Basic principle of water splitting by photocatalysts	34
Figure 1.14	Color of dye after and before degradation	38
Figure 2.1	Schematic representation for synthesis Cu, Cu <sub>2</sub> O and Cu/Cu <sub>2</sub> O	54
Figure 2.2	Powder x-ray diffraction pattern of copper oxalate nanorods (CuC <sub>2</sub> O <sub>4</sub> .H <sub>2</sub> O) obtained from reverse micelle method {inset shows x-ray line broadening of (110) reflection}	58

<b>Figure No.</b>	<b>Figure Captions</b>	<b>Page No.</b>
Figure 2.3	Powder x-ray diffraction pattern of copper nanoparticles {inset shows x-ray line broadening of (111) reflection}	59
Figure 2.4	Powder x-ray diffraction pattern of Cu <sub>2</sub> O synthesized at 850 °C and 350°C.	60
Figure 2.5	Powder X-ray diffraction pattern of CuO heated in Argon at different temperatures	60
Figure 2.6	Powder x-ray diffraction pattern of Cu/Cu <sub>2</sub> O nanocomposites	62
Figure 2.7	Thermogravimetric analysis of copper oxalate nanorods (inset DTG)	63
Figure 2.8:	Differential scanning calorimetry of copper oxalate nanorods	64
Figure 2.9	FESEM micrograph of copper nanoparticles.	64
Figure 2.10	FESEM micrograph of Cu <sub>2</sub> O synthesized at 850 °C at two magnifications	65
Figure 2.11	FESEM micrograph of Cu <sub>2</sub> O synthesized at 350 °C at two magnifications	65
Figure 2.12	TEM micrograph of Cu/Cu <sub>2</sub> O nanocomposites (a) low (b) high magnification	66
Figure 2.13	TEM micrograph of copper oxalate nanorods	67
Figure 2.14	TEM micrograph of copper nanoparticles	67
Figure 2.15	HRTEM micrograph of copper nanoparticles	68
Figure 2.16	TEM micrograph of Cu <sub>2</sub> O synthesized at 850 °C	69
Figure 2.17	TEM micrograph of Cu <sub>2</sub> O synthesized at 350 °C	69

<b>Figure No.</b>	<b>Figure Captions</b>	<b>Page No.</b>
Figure 2.18	TEM micrograph of Cu/Cu <sub>2</sub> O nanocomposites (a) low (b) high magnification	70
Figure 2.19	XPS spectra of Cu nanoparticles	70
Figure 2.20	Diffuse reflectance spectra of Cu <sub>2</sub> O	71
Figure 2.21	Cyclic voltammogram (HER) of copper, cuprous oxide nanoparticles and copper/cuprous oxide nanocomposites (current)	73
Figure 2.22	Cyclic voltammogram (HER) of copper, cuprous oxide nanoparticles and copper/cuprous oxide nanocomposites (current density)	74
Figure 2.23	Cyclic voltammogram (OER) of copper, cuprous oxide nanoparticles and copper/cuprous oxide nanocomposites (current)	75
Figure 2.24	Cyclic voltammogram (OER) of copper, cuprous oxide nanoparticles and copper/cuprous oxide nanocomposites (current density)	76
Figure 2.25	Powder x-ray diffraction pattern of copper nanoparticles (after HER and OER)	78
Figure 2.26	TEM micrograph of copper nanoparticles (after HER)	79
Figure 2.27	HRTEM micrograph of copper nanoparticles (after HER)	79
Figure 2.28	TEM micrograph of copper nanoparticles (after OER)	80
Figure 2.29	HRTEM micrograph of copper nanoparticles (after OER)	80
Figure 2.30	Adsorption of Methylene blue with Cu <sub>2</sub> O	81

<b>Figure No.</b>	<b>Figure Captions</b>	<b>Page No.</b>
Figure 2.31	Photodegradation of Methylene blue with Cu <sub>2</sub> O synthesized at 850 °C (a) with light and with H <sub>2</sub> O <sub>2</sub> (b) with light and without H <sub>2</sub> O <sub>2</sub> (c) without light and with H <sub>2</sub> O <sub>2</sub>	83
Figure 2.32	Photodegradation of Methylene blue with Cu <sub>2</sub> O synthesized at 350 °C (a) with light and with H <sub>2</sub> O <sub>2</sub> (b) with light and without H <sub>2</sub> O <sub>2</sub> (c) without light and with H <sub>2</sub> O <sub>2</sub>	84
Figure 2.33	Photodegradation of methylene blue using (a) Cu <sub>2</sub> O – 850 °C (b) Cu <sub>2</sub> O – 350 °C	85
Figure 2.34	HRTEM micrograph of (a) Cu <sub>2</sub> O – 850°C (b) Cu <sub>2</sub> O – 350 °C	86
Figure 2.35	Recyclability of Cu <sub>2</sub> O – 850 °C as a photocatalyst (5 cycles)	87
Figure 2.36	Percentage degradation of methylene blue after 120 min of Cu <sub>2</sub> O – 850 °C	87
Figure 2.37	Plot of Absorbance vs Time where Cu <sub>2</sub> O – 850 °C is used as photocatalyst during degradation of dye with light with H <sub>2</sub> O <sub>2</sub> (Inset shows the plot of ln(Abs.) vs Time)	88
Figure 3.1:	General procedure of Cu/Cu <sub>2</sub> O nanocomposites synthesis	101
Figure 3.2	Powder X-ray diffraction patterns of Cu/Cu <sub>2</sub> O nanocomposites obtained by hydrothermal method at different hydrothermal reaction time	104
Figure 3.3	Transmission electron micrograph of Cu/Cu <sub>2</sub> O nanocomposites obtained by hydrothermal method after (a) 24 h (b) 72 (c, d) 120 h	106

<b>Figure No.</b>	<b>Figure Captions</b>	<b>Page No.</b>
Figure 3.4	High resolution transmission electron micrograph of Cu/Cu <sub>2</sub> O nanocomposites obtained by hydrothermal method after hydrothermal reaction time of 120 h	107
Figure 3.5	Adsorption - desorption isotherms of Cu/Cu <sub>2</sub> O nanocomposites obtained by hydrothermal method after hydrothermal reaction time of 24 and 120 h	109
Figure 3.6	Diffuse reflectance spectra of Cu/Cu <sub>2</sub> O nanocomposites	110
Figure 3.7	Cyclic voltammogram of entire Cu/Cu <sub>2</sub> O nanocomposites	112
Figure 3.8:	Electrical impedance spectra of Cu/Cu <sub>2</sub> O nanocomposites: Nyquist plot	115
Figure 4.1	Powder X-ray diffraction pattern of CuO	131
Figure 4.2	FESEM micrograph of (a, b) pure micron and (c, d) pure nano sized CuO	133
Figure 4.3	FESEM micrograph of nano-micron composites of CuO (a) 20 % (b) 40 % (c) 50 % (d) 60 %	134
Figure 4.4	TEM micrograph of (a) pure micron (b) pure nano-sized CuO	135
Figure 4.5	(a) TEM (b) HRTEM micrograph of pure nano-sized CuO particles	136
Figure 4.6:	TEM micrograph of nano-micron composites of CuO (a) 20 % (b) 40 % (c) 50 % (d) 80 %	137
Figure 4.7	Diffuse reflectance spectra of CuO composites	140
Figure 4.8	Cyclic voltammogram of CuO nanocomposites	141

<b>Figure No.</b>	<b>Figure Captions</b>	<b>Page No.</b>
Figure 4.9	Cyclic voltammogram of CuO nanocomposites (current density on ESA)	143
Figure 4.10	Magnetization vs temperature of CuO	145
Figure 4.11	Magnetization vs magnetic field of CuO at 5 K (inset show the magnetization at low field)	146
Figure 4.12	Magnetization vs magnetic field of CuO at 10 K (inset shows the low field magnetization)	147
Figure 4.13	Magnetization vs magnetic field of CuO at 300 K (inset shows magnetization data at low field)	148
Figure 4.14	Coercivity vs weight percentage of nanoparticles in nano-micron composites	149
Figure 5.1	Powder x-ray diffraction pattern of cobalt oxalate nanorods ( $\text{CoC}_2\text{O}_4 \cdot 2\text{H}_2\text{O}$ )	163
Figure 5.2:	Powder x-ray diffraction pattern of cobalt nanoparticles obtained by decomposition of copper oxalate at different heating and cooling rate	164
Figure 5.3	Thermogravimetric analysis of cobalt oxalate nanorods (inset DTG)	165
Figure 5.4	Differential scanning calorimetry of cobalt oxalate nanorods	166
Figure 5.5	FESEM micrograph of cobalt oxalate nanorods	167
Figure 5.6	TEM micrograph of cobalt oxalate nanorods	167
Figure 5.7	FESEM micrograph of cobalt nanoparticles at different heating and cooling rates	168

<b>Figure No.</b>	<b>Figure Captions</b>	<b>Page No.</b>
Figure 5.8	TEM micrograph of cobalt nanoparticles at different heating and cooling rates	168
Figure 5.9	Cyclic voltammogram (HER) of cobalt nanoparticles	170
Figure 5.10	Cyclic voltammogram (OER) of cobalt nanoparticles	171
Figure 5.11	Electrical impedance spectra of cobalt nanoparticles: Nyquist plot	173
Figure 5.12	Plot of magnetization vs magnetic field of Co nanoparticles (100 K)	175
Figure 5.13	Plot of magnetization vs magnetic field of Co nanoparticles (300 K)	176
Figure 6.1	Schematic diagram of synthesis of $\text{CoFe}_2\text{O}_4$ nanoparticles	188
Figure 6.2	Schematic diagram for synthesis of $\text{BaTiO}_3$ nanoparticles	189
Figure 6.3	Schematic diagram for synthesis of $\text{BaTiO}_3/\text{CoFe}_2\text{O}_4$ heterostructures (CS1 & CS2)	190
Figure 6.4	Schematic diagram for synthesis of $\text{BaTiO}_3/\text{CoFe}_2\text{O}_4$ heterostructures (CS3 & CS4)	191
Figure 6.5	Powder X-ray diffraction patterns of $\text{CoFe}_2\text{O}_4$ obtained by (a) Coprecipitation (b) Hydrothermal method.	194
Figure 6.6	Powder X-ray diffraction patterns of $\text{BaTiO}_3$ obtained by hydrothermal process using (a) $\text{TiO}_2$ (b) Titanium isopropoxide as Ti precursor	195

<b>Figure No.</b>	<b>Figure Captions</b>	<b>Page No.</b>
Figure 6.7	Powder X-ray diffraction patterns of brown precipitate at 80 °C	196
Figure 6.8	Powder X-ray diffraction patterns of CS1 at 650 °C and CS2 at 180 °C	197
Figure 6.9	Powder X-ray diffraction patterns of CS3 and CS4	198
Figure 6.10	FESEM micrograph of CoFe <sub>2</sub> O <sub>4</sub> nanoparticles obtained by coprecipitation (a, b) and hydrothermal route (c, d)	199
Figure 6.11	FESEM micrograph of BaTiO <sub>3</sub> nanoparticles obtained by hydrothermal route using (a) TiO <sub>2</sub> and (b) titanium isopropoxide as source of Ti.	200
Figure 6.12	FESEM micrograph of BaTiO <sub>3</sub> /CoFe <sub>2</sub> O <sub>4</sub> (CS1) heterostructures obtained by coprecipitation route after heating at (a) 80 °C and (b) 650 °C	201
Figure 6.13	FESEM micrograph of BaTiO <sub>3</sub> /CoFe <sub>2</sub> O <sub>4</sub> (CS2) heterostructures obtained by hydrothermal route at 180 °C	201
Figure 6.14	FESEM micrograph of BaTiO <sub>3</sub> /CoFe <sub>2</sub> O <sub>4</sub> (CS3 & CS4) heterostructures obtained by in-situ hydrothermal route at 180 °C using (a) TiO <sub>2</sub> (b) titanium isopropoxide as Ti source	202
Figure 6.15	TEM micrograph of CoFe <sub>2</sub> O <sub>4</sub> nanoparticles by (a) coprecipitation at 650 °C and (b) hydrothermal route at 180 °C	203
Figure 6.16	HRTEM micrograph of CoFe <sub>2</sub> O <sub>4</sub> nanoparticles obtained by (a) coprecipitation at 650 °C and (b) hydrothermal route at 180 °C	204

<b>Figure No.</b>	<b>Figure Captions</b>	<b>Page No.</b>
Figure 6.17	TEM micrograph of BaTiO <sub>3</sub> nanoparticles obtained by hydrothermal route at 180 °C (a) TiO <sub>2</sub> and (b) titanium isopropoxide source	204
Figure 6.18	TEM micrograph of BaTiO <sub>3</sub> /CoFe <sub>2</sub> O <sub>4</sub> (CS1) heterostructures obtained by coprecipitation route at 650 °C	205
Figure 6.19	TEM micrograph of BaTiO <sub>3</sub> /CoFe <sub>2</sub> O <sub>4</sub> (CS2) heterostructures obtained by hydrothermal route at 180 °C	206
Figure 6.20	HRTEM micrograph of BaTiO <sub>3</sub> /CoFe <sub>2</sub> O <sub>4</sub> (CS2) heterostructures obtained by hydrothermal route at 180 °C	207
Figure 6.21	TEM micrograph of BaTiO <sub>3</sub> /CoFe <sub>2</sub> O <sub>4</sub> (CS3) heterostructures obtained by in-situ hydrothermal route at 180 °C using TiO <sub>2</sub> as titanium source	207
Figure 6.22	HRTEM micrograph of BaTiO <sub>3</sub> /CoFe <sub>2</sub> O <sub>4</sub> (CS3) heterostructures by in-situ hydrothermal route at 180 °C using TiO <sub>2</sub> as titanium source	208
Figure 6.23	TEM micrograph of BaTiO <sub>3</sub> /CoFe <sub>2</sub> O <sub>4</sub> (CS4) heterostructures obtained by in-situ hydrothermal route at 180 °C using titanium isopropoxide as titanium source	209
Figure 6.24	HRTEM micrograph of BaTiO <sub>3</sub> /CoFe <sub>2</sub> O <sub>4</sub> (CS4) heterostructures obtained by in-situ hydrothermal route at 180 °C using titanium isopropoxide as titanium source	210

<b>Figure No.</b>	<b>Figure Captions</b>	<b>Page No.</b>
Figure 6.25	Plot of magnetization with magnetic field of $\text{CoFe}_2\text{O}_4$ at (a) 100 and (b) 300 K	212
Figure 6.26	Plot of magnetization with magnetic field of CS1 and CS2 at (a) 100 (b) 300 K	213
Figure 6.27	Plot of magnetization with magnetic field of CS3 and CS4 at 100 & 300 K	214
Figure 7.1	Powder x-ray diffraction pattern of particles synthesized by (a) solid state (SS) and (b) reverse micellar (RM) route	230
Figure 7.2	Rietveld refined x-ray diffraction pattern of synthesized particles of $\text{La}_{0.82}\text{Sr}_{0.18}\text{MnO}_3$ by solid state route	231
Figure 7.3	Powder x-ray diffraction pattern of nano-micron composites of $\text{La}_{0.82}\text{Sr}_{0.18}\text{MnO}_3$	232
Figure 7.4	Transmission electron micrograph of (a) micron size (b) nano size particles of $\text{La}_{0.82}\text{Sr}_{0.18}\text{MnO}_3$	233
Figure 7.5	Field emission scanning electron micrograph of $\text{La}_{0.82}\text{Sr}_{0.18}\text{MnO}_3$ nano-micron composites (0.0, 0.5, 1, 2, 3 and 5 %)	234
Figure 7.6	FESEM micrograph of $\text{La}_{0.82}\text{Sr}_{0.18}\text{MnO}_3$ nano-micron composites (0.0, 0.5, 1, 2, 3 and 5.0 %)	235
Figure 7.7	Figure 6.7: Cross-sectional FESEM micrograph of $\text{La}_{0.82}\text{Sr}_{0.18}\text{MnO}_3$ nano-micron composites (0.0, 0.5, 1, 2, 3 and 5 %)	236

<b>Figure No.</b>	<b>Figure Captions</b>	<b>Page No.</b>
Figure 7.8	SEM-EDAX micrograph of pure micron and nano $\text{La}_{0.82}\text{Sr}_{0.18}\text{MnO}_3$ particles	238
Figure 7.9	Plot of density (●) and surface area (◆) with weight % addition of nanoparticles	241
Figure 7.10	Plot of magnetization with temperature of entire $\text{La}_{0.82}\text{Sr}_{0.18}\text{MnO}_3$ .	242
Figure 7.11	Plot of magnetization with magnetic field of $\text{La}_{0.82}\text{Sr}_{0.18}\text{MnO}_3$ .	243

## List of Table

S. No.	Title	Page No.
Table 1.1	Nanoparticles synthesis methodology	5
Table 1.2	Different surfactant with their molecular formula and abbreviations	13
Table 3.1	Weight percentage of Cu and Cu <sub>2</sub> O obtained after reaction for varying time in Cu/Cu <sub>2</sub> O nanocomposites	105
Table 3.2	Morphology, particle size and surface area of Cu/Cu <sub>2</sub> O nanocomposites	108
Table 3.3	HER and OER currents and current density	113
Table 3.4	Sonogashira cross coupling yield using different catalysts	116
Table 4.1	weight fraction of micron sized CuO and copper oxalate in nano-micron composites of CuO	117
Table 4.2	Particles size, density and surface area nano-micron CuO composites	138
Table 4.3	Electroactive surface area, current and current density of nano-micron composites of CuO	144
Table 5.1	Particle size and surface area of synthesized Co nanoparticles	169
Table 5.2	Peak potential separation and currents for HER & OER of Co nanoparticles synthesized from cobalt oxalate at various rates of heating and cooling during decomposition in 10%H <sub>2</sub> /argon atmosphere	172
Table 5.3	Magnetization values of Co nanoparticles	176

<b>S. No.</b>	<b>Title</b>	<b>Page No.</b>
Table 6.1	Lattice parameter of BaTiO <sub>3</sub> @CoFe <sub>2</sub> O <sub>4</sub> heterostructures	198
Table 6.2	Particles size and surface area of BaTiO <sub>3</sub> (BT1, BT2), CoFe <sub>2</sub> O <sub>4</sub> (CF1, CF2) & BaTiO <sub>3</sub> @CoFe <sub>2</sub> O <sub>4</sub> (CS1, CS2, CS3, CS4)	211
Table 6.3	Saturation magnetization, remnant magnetization and coercivity for CF1, CF2, CS1, CS2, CS3 and CS4 at 100 & 300 K	215
Table 7.1	weight fraction of micron and nano sized La <sub>0.82</sub> Sr <sub>0.18</sub> MnO <sub>3</sub> in nano-micron composites of La <sub>0.82</sub> Sr <sub>0.18</sub> MnO <sub>3</sub>	227
Table 7.2	Refined positional and thermal parameters for La <sub>0.82</sub> Sr <sub>0.18</sub> MnO <sub>3</sub> at 1050 °C synthesized by solid route, relative position along c axis (z), occupation number (n) and isotropic thermal factor (U <sub>iso</sub> ). The numbers in parentheses are the estimated standard deviations in the last digit.	232
Table 7.3	Elemental analysis from SEM-EDAX for SS (pure micron) and RM (pure nano) route synthesized compound	237
Table 7.4	Properties of La <sub>0.82</sub> Sr <sub>0.18</sub> MnO <sub>3</sub> Solid State Route (SS) and Reverse Micelle Route (RM) synthesized compound and their nano-micron composites	240

## Abbreviations and Symbols

Å	Angstroms
°C	Centigrade
µm	Micrometer
nm	Nanometer
min	Minutes
h	Hours
s	Seconds
µE	Microemulsion
PXRD	Powder X-ray diffraction
TEM	Transmission Electron Microscopy
HRTEM	High Resolution Transmission Electron Microscopy
FESEM	Field Emission Scanning Electron Microscopy
EDAX	Energy Dispersive X-ray Analysis
DRS	Diffuse reflectance spectroscopy
BET	Brunauer – Emmett – Teller
VB	Valence band
CB	Conduction band
NHE	Normal hydrogen electrode
CTAB	Cetyl trimethylammonium bromide
UV-vis	Ultraviolet -visible
MB	Methylene blue
Ms	Saturation Magnetization
Mr	Remnant Magnetization

Oe	Oersted
HER	Hydrogen evolution reaction
OER	Oxygen evolution reaction
ESA	Electroactive surface area
emu	Electro magnetic unit